HIGH FUNDAMENTAL FREQUENCY PM SYNCHRONOUS MOTOR DESIGN NEURAL REGRESSION FUNCTION

Adel EL SHAHAT
Department of Electrical and Computer Engineering,
Caldwell Lab, 205 Dreese Labs, 2015 Neil Ave. Columbus Ohio 43210,
Ohio State University, USA. E-mail: adel.elshahat@ieee.org; ahmed.210@osu.edu

Hamed EL SHEWY
Department of Electrical Power and Machines Engineering,
Faculty of Engineering, Zagazig University,
Zagazig, Egypt. E-mail: prof.hamed_elshewy@yahoo.com

Abstract: *This paper proposes high fundamental frequency permanent magnet synchronous machine design with the suitable machine materials. The final design offers significant reductions in both weight and volume in a power range of 5:500 Kw. A rotor length to diameter ratio is used as an important design parameter. The results are depicted by 3D plot figures for a number of machines sizing. The simulation of generators sizing is performed using MATLAB. Then, this paper introduces three neural network units. Finally, deduction of algebraic nonlinear function which, connects between inputs and outputs for neural network is presented to be used without training each time.*

Key words: *Design, High Frequency, Permanent Magnet, Synchronous Motor, Neural Network and MATLAB.*

1. Introduction

High frequency PM machines can find application in various fields, such as energy storage flywheel, aircraft generator, and milling spindle. It is quite different to design such a high frequency machine from designing a common machine with low speed and low frequency. So, more attention has been paid to the development of high fundamental frequency PM generators driven by micro-turbines, as prime movers with local conversion at load points [1]. For high-frequency applications, the rotor aspect ratio, defined as length-to-diameter, is a critical parameter. Stator core losses may be minimized by using laminated steel in stator construction and by not generating frequencies that are too high. The main applications of PMSG are for power generation as part of renewable energy resources and main generators for aircraft, etc. [2-9]. The sizing of HFPMSG design must address system topology for good power/volume, low cost, and superior efficiency [1-14]. The influence of the choice of stator lamination material on iron loss in a high speed, high power, and permanent magnet generator is investigated. The ability of the ANN to approximate nonlinear functions with Dynamic Back-Propagation (DBP) has gained a great attention [22-27]. This paper presents general the sizing of HFPMSGs for the power range of 5:500 Kw, with various tip speeds of 50:250 m/s. Then, four neural networks (Basic, Geometric, Electric) with their regression functions are presented.

2. Basic Selections

2.1. Permanent Magnets

The rare earth magnets, SmCo and NdFeB, have become popular because of their greater power density, high Coercivity, high flux densities, and the linearity of their demagnetization curves [13], [15]. NdFeB is preferred because it is cheaper and more readily available. Therefore, NdFeB magnets are selected for use in PMG, with some conservatively assumed values [14].

2.2. Stator and Rotor Material

The rotor is usually built from the same material as the stator for ease of construction, but it can be made of any economical steel, provided it is strong enough for its function [13], [16]. TM19, 29 gauge electrical silicon steel is selected for the PMG because it is economical, its thin laminations minimize power losses due to the circulating eddy current, and because it has a saturation flux density of about 1.8 T [13], [14].

3. Machine Design Parameters

3.1. Stator Mechanical Design

The stator is an important part of the machine because it serves as the main structural component, it

provides the housing for the armature windings, and it completes the flux path for the magnetic circuit. Slotted stators are the traditional stator design and consist of openings around the stator for the armature windings, as shown in Figure 1 (a).

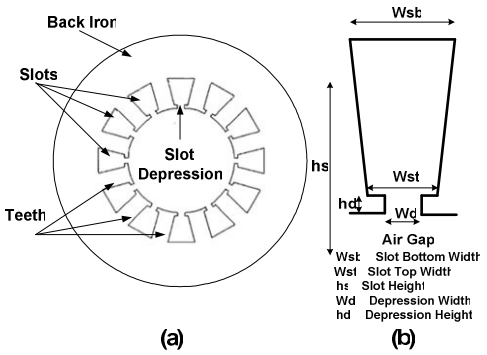

Fig.1 (a) Slotted Stator; (b) Stator Slot Geometry.

In this paper, the slots are trapezoidal, but assumed to be approximately rectangular, as shown in Figure 1 (b). They contain form-wound windings so that the depression width is the same as the top slot width. Slotting is used because of its advantages, such as the achievement of a narrow air gap length to maximize the flux linkage, the increase in surface contact area between the windings, and a path of low thermal resistance, provided by stator steel for good heat conduction [14]. The initial design of the generator assumes a three-phase machine. Also, a 36 slots machine is chosen for the initial generator design [13].

3.2. Rotor Mechanical Design

The surface mounted permanent magnets in the rotor as shown in fig. 2 are selected here due to its suitability for high speed applications.

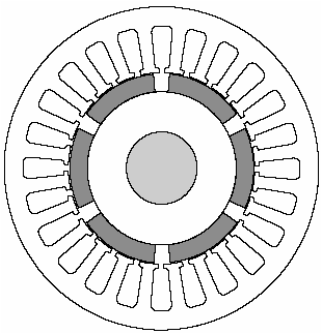

Fig. 2 Surface Mounted PM in the rotor.

For high-speed applications, the rotor aspect ratio, defined as length-to-diameter (L/D), is a critical parameter. PM machines offer flexibility in selecting pole sizes, which allows for smaller diameters. A normal L/D ratio for a wound rotor machine is 0.5 – 1.0, compared to 1 – 3 for a PM machine [17]. So, here it is selected to be 2.5. The rotor radius and rotational speed also determine the tip speed of the machine, which is the surface velocity of the rotor.

$$v_{tip} = r\omega_m \quad (1)$$

where ω_m: angular speed (rad/sec); r: rotor radius (m)

The upper limit on tip speed is between 100-250 m/s, depending on the design of the of machines. In this design, a range of tip speed is taken to be (50:250).

3.3. Number of Poles and Magnets Pole Design

An even number of poles is always used, here P = 3, because this provides a balanced rotational design. Assuming a constant mechanical rotation speed, electrical frequency is given as.

$$N(2P) = 120f \quad (2)$$

N: speed (rpm); P: pole pairs; f: elect. frequency (Hz)

If a PM generator is going to be the source of DC bus through a rectifier system, a high pole number is desirable because as the electrical frequency increases, support components such as filter capacitors and inductors can be much smaller. Therefore, for a given rotational speed, one cheap and efficient solution is to have a higher number of pole pairs and frequency. However, as the frequency increases, higher stator losses result because core losses are proportional to frequency squared. In addition, as the pole number gets larger, the number of slots per pole per phase decreases and can cause the voltage waveforms to become less sinusoidal so all factors must be considered. The pole arc of the magnets can also be varied. Magnets seldom span the full pole pitch because the flux at the transition between north and south poles leaks between poles without linking the coils in the stator. The gaps between the poles usually contain non – magnet pieces, such as soft iron, so that no flux crosses over the air gap between magnets. All full pole arc is $\Theta_{me} = 180\ ^{o}E$ and produces a full voltage waveform but has increased harmonic content. As the pole arc is reduced (up to 20 – 30 %) and those areas are filled in with soft – iron pieces, the resulting flux waveform is more sinusoidal and has fewer harmonics and therefore lower rotor losses. The magnet poles are sometimes skewed to

reduce cogging torque and smooth out variations in air gap reluctance, flux, and voltage waveforms. Skewing of magnets occurs axially along the length of the rotor to provide a constant rotational torque and prevent pole pieces from exactly lining up with stator teeth. Magnet poles skew factor is selected to reduce cogging torque and smooth out variations in air gap reluctance, flux, and voltage waveforms.

$$k_{sn} = \frac{\sin(n\theta_s)}{\frac{\theta_s}{2}} \quad (3)$$

where θ_s: Skew angle, rad E; n: Harmonic number

3.4. Magnetic Dimensions

The magnetic dimensions that affect a PM machine are air gap and magnet height. The air gap flux density (Bg) can be represented by Equation 4. The radial air gap is made as small as possible to maximize the air gap flux density, minimize the flux leakage, and to produce a lower reluctance value.

$$B_g = \frac{h_m}{h_m + g} B_r \quad (4)$$

where h_m: Magnet height (mm); g: Air gap (mm); B_r: Magnet Remnant Flux Density (T)

Magnets losses are reduced, using smaller magnets. For uniform magnetic fields, the magnet height is usually larger than the air gap, by a factor 5 – 10.

3.5. Slots Per Pole, Per Phase

Three-phase machines are typically used in this study as the standard choice for most motors and generators. Another important design parameter is the number of slots per pole, per phase (m), as in Equation 5.

$$m = \frac{N_s}{2 * P * q} \quad (5)$$

Varying the number of slots/pole/phase is used to produce a more sinusoidal voltage waveform and reduce machine harmonics.

3.6. Stator Windings

The pitch of a winding (α) refers to the angular displacement between the sides of a coil. The breadth of a stator winding results from the coils occupying a distribution of slots within a phase belt. In smaller machines, coils are composed of round insulated wires that are placed in the stator slot, along with insulation material. A slot fill factor (λ_s) is used to determine how much of the slot's cross-sectional area is occupied by winding material, as in Equation 6.

$$\lambda_s = \frac{Winding \quad Area}{Total \quad Slot \quad Area} \quad (6)$$

Typically, machines contain two coils sides per slot, making the winding a double-layer design [13]. Overall, slot fill factors vary in value from 0.3 – 0.7, depending on the number and size of the conductors in the slots, as well as the amount of labor utilized. In this paper, a slot fill factor of 0.5 is assumed. Almost all machines use series, wye – connected windings because they provide the safest alternative. Therefore, wye series connected windings are selected for use in the designs in this study.

3.7. Machine Calculated Parameters

Each phase of the machine is modeled, as shown in Figure 3.

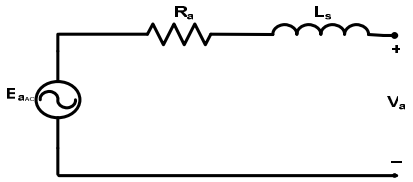

Fig.3 A Per Phase Electrical Model.

R_a: Armature resistance; L_s: Synchronous inductance; E_a: Back e.m.f voltage and V_a : Terminal voltage.

3.8. Winding Resistances

The resistance of copper phase windings is calculated in Equation 7

$$R_a = \frac{l}{\sigma * A_{ac}} \quad (7)$$

where l: length of conductor; σ: winding conductivity; A_{ac}: winding cross – sectional area

$$A_{ac} = \frac{A_s * \lambda_s}{2 * N_C} \quad (8)$$

where A_s: slot Area, N_c: turns per coil

But the above stator resistance equation may be used as in low frequencies applications, so it has to be developed. Since the machine rotates at high speed, and high frequency and so the skin depth may be affected. In conductors that carry high frequency currents, skin effect can become an issue and affect the operation of the machine. Skin effect is caused by eddy currents in the windings themselves due to the changing magnetic field. These eddy currents force the current flowing in the conductor to crowd to the outer

edges of the conductor. This in turn causes the current to flow through a smaller cross – sectional area and increase the resistance of the conductor.

It is well known that, when conductive material is exposed to an ac magnetic field, eddy currents are induced in the material in accordance with Lenz's law. The power loss resulting from eddy currents which can be induced in the slot conductors appears as an increased resistance in the winding. To understand this phenomenon, let us consider a rectangular conductor as shown in fig. 4. The average eddy current loss in the conductor due to a sinusoidal magnetic field in the *y* direction is given approximately by Hanselman [12].

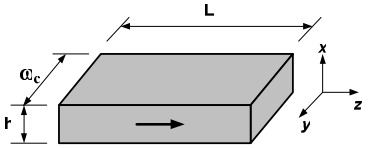

Fig. 4 Rectangular Conductor Geometry.

$$P_{ec} = \frac{1}{12}\sigma L \omega_c h^3 \omega^2 u_0^2 H_m^2 \qquad (9)$$

H_m: turn field intensity value; u_0: perm. of free space. Since skin depth is defined as

$$\delta = \sqrt{\frac{2}{\omega u_0 \sigma}} \qquad (10)$$

Equation (9) can be written as

$$P_{ec} = \frac{L\omega_c h^3}{6\sigma\delta^4} H_m^2 \qquad (11)$$

Using this expression it is possible to compute the ac resistance of the slot conductors. If the slot conductors are distributed uniformly in the slot, and substituting the field intensity into eq. (11) and summing over all ns conductors gives a total slot eddy current loss of

$$P_e = (\frac{d_s L h^2 n_s^2}{9\sigma\delta^4 \omega_s}) I^2 \qquad (12)$$

where I is the rms conductor current; ω_s: Slot width(m); d_s: Slot depth(m)

The slot resistance of a single slot containing n_s conductors connected in series is

$$R_{sl} = \frac{\rho n_s^2 L}{k_{cp}\omega_s d_s} \qquad (13)$$

where L: the slot length; k_{cp}: the conductor packing factor, is the ratio of cross sectional area occupied by conductors to the entire slot area and ρ: electrical resistivity (Ω.m).

Using eq. (13), the total slot resistance can be written as

$$R_{st} = R_{sl} + R_{ec} = R_{sl}(1+\Delta_e) \qquad (14)$$

In this equation, $\Delta_e = R_{ec}/R_{sl}$ is the frequency-dependent term. Using eq. (13) and eq. (12), this term simplifies to

$$\Delta_e \equiv \frac{R_{ec}}{R_{sl}} = \frac{1}{9}(\frac{d_s}{\delta})^2 (\frac{h}{\delta})^2 \qquad (15)$$

This result shows that the resistance increases not only as a function of the ratio of the conductor height to the skin depth but also as a function of the slot depth to the skin depth. Thus, to minimize ac losses, it is desirable to minimize the slot depth as well as the conductor dimension. For a fixed slot cross-sectional area, this implies that a wide but shallow slot is best.

3.9. Winding and Magnet Factors

Winding are short-pitched and have breadth associated with them. To account for these effects, a winding factor (k_w) is utilized, as in Equation 16.

$$k_{wn} = k_{pn} * k_{bn} \qquad (16)$$

Short-pitching is an important means for eliminating harmonics and improving the power quality of the machine. The pitch factor is shown in Equation 17.

$$k_{pn} = \sin(\frac{n*\alpha}{2}) * \sin(\frac{n*\pi}{2}) \qquad (17)$$

The breadth factor explains the effect of the windings occupying a distribution or range of slots within a phase belt. The breadth factor is derived in Eq. 18.

$$k_{bn} = \frac{\sin(\frac{n*m*\gamma}{2})}{m*\sin(\frac{n*\gamma}{2})} \qquad (18)$$

m: slots per pole per phase; γ: coil electrical angle

The magnetic flux factor equation [12], for the slotted stator and surface magnet configuration is shown in Equation 19.

$$k_{gn} = \frac{R_i^{np-1}}{R_s^{2np} - R_i^{2np}} * [(\frac{np}{np+1}) * (R_2^{np+1} - R_1^{np+1}) + \frac{np}{np-1} * R_s^{2np} * (R_1^{1-np} - R_2^{1-np})] \qquad (19)$$

where R_s: outer magnetic boundary, R_2: outer boundary of magnet; R_i: inner magnetic boundary, R_1: inner boundary of magnet

3.10. Flux and Voltage

For useful voltage, only the fundamental components are used to determine the internal voltage (back e.m.f) of the generator, as shown in Eq.s 20, 21, and 22.

$$E_a = \omega_0 \lambda \qquad (20)$$

$$\lambda = \frac{2*R_s*L_{st}*N_a*k_w*k_s*B_1}{P} \qquad (21)$$

$$B_1 = \frac{4}{\pi} * B_g * k_g * \sin(\frac{P\theta_m}{2}) \quad (22)$$

where θ_m: magnet physical angle

$$B_g = \frac{k_l C_\phi}{1 + k_r * \frac{u_{rec}}{PC}} * B_r \quad (23)$$

where u_{rec}: recoil permeability; B_r: remnant flux density

$$PC = \frac{h_m}{g_e * C_\phi} \quad (24)$$

PC: permeance coeff.; C_Φ: flux concentration factor

$$N_a = 2 * P * N_c \quad (25)$$

where N_c : Turns per coil; N_a : Number of armature turns (each slot has 2 half coils)

$$\tau_s = w_s + w_t; g_e = k_c * g \quad (26)$$

where g_e: effective air gap; w_s: average slot width; w_t: tooth width

Here, a leakage factor (Kl ~ 0.95) and a reluctance factor (Kr~1.05) are both used for surface magnets. The presence of the slots in the stator also affects the air gap flux density because of the difference in permeance caused by the slots. Carter's coefficient (kc) is used to account for this effect [12].

$$k_c = [1 - \frac{1}{\frac{\tau_s}{w_s} * (5 * \frac{g}{w_s} + 1)}]^{-1} \quad (27)$$

The vector relationship is depicted in Figure 5. The terminal voltage (V_a) is calculated from the internal voltage (E_a), and the synchronous reactance voltage drop. The armature resistance is usually ignored because it is much smaller than synchronous reactance. The voltage is found as a relation in output power (P_{wr}), e.m.f, and reactance from the resulting quadratic equation.

$$V_a = \sqrt{\frac{-BB + \sqrt{BB^2 - 4CC}}{2}} \quad (28)$$

$$BB = \frac{2}{3} X_s P_{wr} - E_a^2; \; CC = \frac{2}{9} X_s^2 P_{wr}^2$$

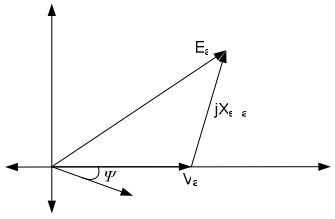

Fig. 5 The Voltage Vector Relationship.

3.11. Machine Inductances

In a slotted PM machine, there are three distinct components of inductance: the largest, air gap inductance slot leakage inductance, and the smallest, end-turn inductance. The total inductance for the phase is the sum of the three inductances, ignoring other small factors.

$$L_s = L_{ag} + L_{slot} + L_e; \quad X_s = \omega_0 * L_s \quad (29)$$

The air gap inductance is given by Eq. 30.

$$L_{ag} = \frac{\lambda}{i} = \frac{q}{2} * \frac{4}{n\pi} * \frac{u_0 * R_s * L_{st} * N_a^2 * k_{wn}^2}{n^2 * P^2 * (g + h_m)} \quad (30)$$

The slot leakage inductance is presented in Equation 31. Assume the slot is rectangular with slot depressions, as in Figure 1, and assume (m) slots per pole per phase, with a standard double layer winding.

$$L_{slot} = L_{as} - L_{am}; (3\,phase) \quad (31)$$

$$L_{am} = 2 * P * L_{st} * Perm * N_{sp} * N_c^2 \quad (32)$$

$$L_{as} = 2 * P * L_{st} * Perm * [4 * N_c^2 (m - N_{sp}) + 2 * N_{sp} * N_c^2] \quad (33)$$

A slot permeance per unit length is shown in Eq. 34.

$$Perm = \frac{1}{3} * \frac{h_s}{w_{st}} + \frac{h_d}{w_d} \quad (34)$$

The end turn inductance is introduced in Equation 35, assuming the end turns are semi-circular, with a radius equal to one-half the mean coil pitch.

$$L_e = \frac{u_0 * N_c * N_a^2 * \tau_s}{2} * \ln(\frac{\tau_s * \pi}{\sqrt{2 * A_s}}) \quad (35)$$

3.12. Basic Losses

Losses in a machine consist of core losses, conductor losses, friction and windage losses, and rotor losses. Rotor losses will be discussed later. Stator core losses, per weight, can be greater than normal in machines because of higher frequencies. These losses are minimized by using laminated steel in stator construction and by not generating frequencies that are too high. Core losses consist of hysteresis and eddy current losses. The best way to approximate core losses is to use empirical loss data. An exponential curve fitting is applied to the empirical data for M-19, 29 gauge material, in order to obtain an equation for estimating core losses, as in Equation 36, with constant values in [19].

$$P_C = P_0 * (\frac{B}{B_0})^{\varepsilon B} * (\frac{f}{f_0})^{\varepsilon f} \quad (36)$$

P_0: Base power; B_0: Base flux density; ε_B: Flux density exponent; f_0: Base frequency; ε_f: Frequency exponent

The conductor losses are found, using Equation 37.

$$P_a = q * I_a^2 * R_a \quad (37)$$

For rotors operating at high speed, the friction and windage in air can cause losses which result in inefficiency and heat production. These losses are

calculated, using the power necessary to overcome the drag resistance of a rotating cylinder, as given by Equation 38 [20].

$$P_{wind} = C_f * \pi * \rho_{air} * \omega^3 * R^4 * L_{st} \quad (38)$$

The coefficient of friction can be approximated by Equation 39.

$$C_f \cong 0.0725 * R_{ey}^{-0.20} \quad (39)$$

where R_{ey}: Reynold's Number

4. Sizing Results

4.1. Machine Initial Sizing

For the basic sizing calculations, an air-cooled generator is assumed with 10 psi [13], [21]. The machine power equation is utilized to derive the rotor radius and stack length of the machine, as in Eq. 40.

$$P_{wr} = 2 * \pi * r * L_{st} * v_{tip} * \tau \quad (40)$$

r : rotor radius; L_{st} : stack length; τ : shear stress (psi)

The L/D ratio is substituted for L_{st}. Using shear stress, rotor tip speed, and machine power rating range, the power equation is calculated to obtain rotor radius and stack length, while matching the desired rotational speed of the machine with a L/D ratio equal to 2.5, as supposed here. Using a pole pair value of 3, a slot height of 10 mm, and a slot fill fraction of 0.5, the frequency is found.

The basic sizing parameters are illustrated in Fig. 6 – 9.

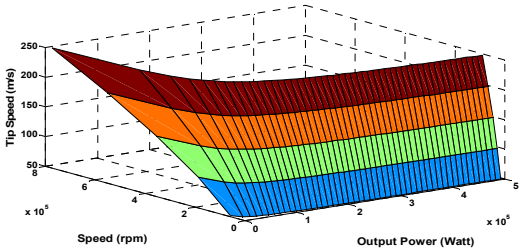

Fig. 6 Power with Speed and Various Tip Speeds.

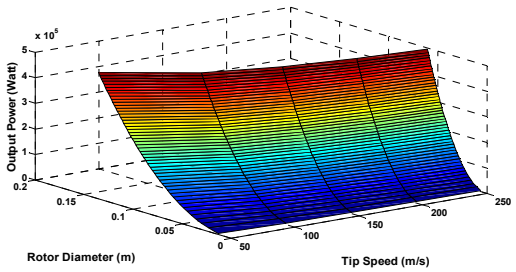

Fig. 7 Power with Rotor Diameter and Tip Speeds.

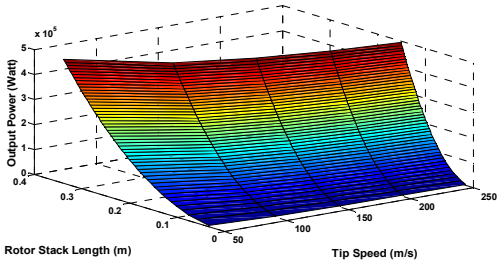

Fig. 8 Power with Rotor Stack Length.

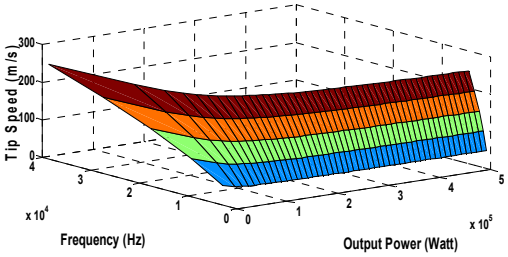

Fig. 9 Power with Frequency and Tip Speeds.

4.2. Detailed Sizing

Once the basic sizing of the machine is complete, in-depth analysis is conducted to obtain the overall performance within the power range of 5: 500 KW generators. Using the equations presented in previous sections, all the detailed parameters can be obtained. The lengths, volumes, masses, and overall generator parameters are calculated, using basic geometric equations and relationships. A 15% service mass fraction is added to the total mass estimate to account for the additional services associated with machines cooling [14], [21]. Once the mass of each of the stator parts is known, core losses are estimated in accordance with them. The calculation of lengths, volumes, and weights are presented. The mass of armature conductors, core mass, magnet mass, and shaft mass are calculated to give the total mass value. Finally, stator resistance, terminal voltage, current, loss types, input power, and efficiency are calculated.

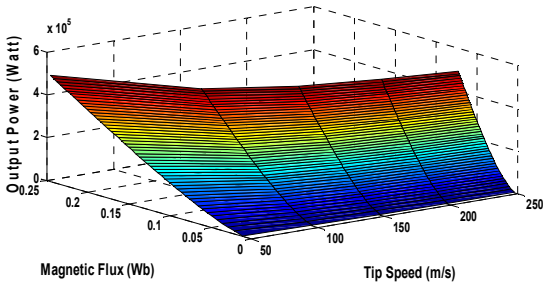

Fig. 10 Power with Magnetic Flux (Wb).

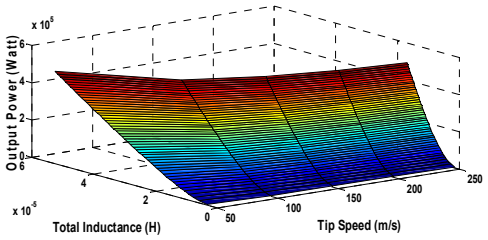

Fig. 11 Power with Total Inductance (H) Relations.

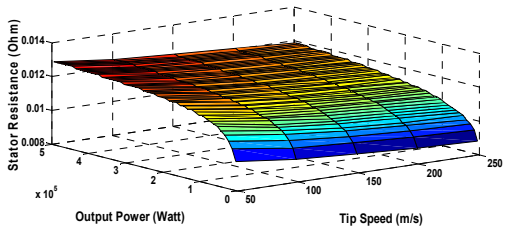

Fig. 12 Power with Stator Resistance Relations.

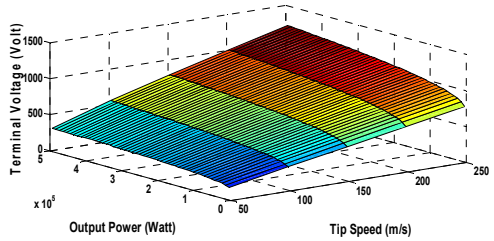

Fig. 13 Power with Terminal Voltage Relations.

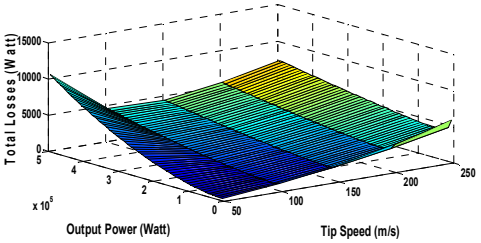

Fig. 14 Output Power with Total Loss Relations.

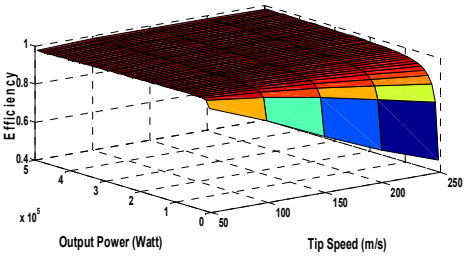

Fig. 15 Output Power with Efficiency Relations.

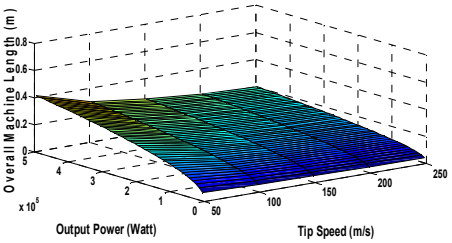

Fig. 14 Power with Overall Machine Length.

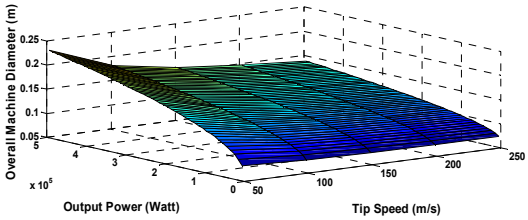

Fig. 16 Power with Overall Diameter Relations.

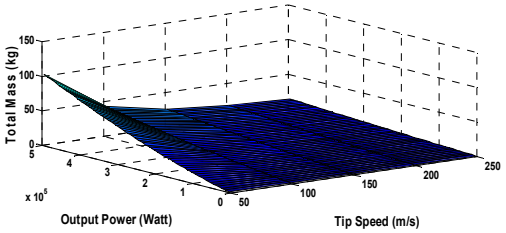

Fig. 17 Power with Total Mass Relations.

5. ANN Models

5.1 ANN Initial Sizing Model

Using the technique as in references [22-27] to implement a neural network unit, this model represents the relations between the required output power and tip speed values as inputs, and the desired rpm speed, the rotor diameter, and the rotor stack length as outputs or targets. This model is done with two layer hidden (contains 8 Neurons) and output (contains 3 Neurons). Then obtaining the algebraic equations as in [27].

$p_{wrn} = (P_{wr} - 250000) / (1.0e+005 *1.4460)$ (41)

$v_{tipn} = (V_{tip} - 150) / (1.0e+005 *0.0007)$ (42)

Equations 41, and 42 present the normalized inputs for output power and tip speed, and the following equations lead to the required derived equation.

$E1= 0.9164 \quad p_{wrn} + \ - 0.5570\ v_{tipn} + 3.8665$

$F1=1 / (1 + \exp (- E1))$ (43)

$E2= 0.1549 \quad p_{wrn} + 0.4871\ v_{tipn} + 6.0496$

$F2=1 / (1 + \exp (-E2))$ (44)

$E3= - 0.0215\ p_{wrn} + - 3.7733\ v_{tipn} + - 1.6948$

$F3=1 / (1 + \exp (- E3))$ (45)

$E4= - 0.0175\ p_{wrn} + - 5.3865\ v_{tipn} + -1.6193$

$F4=1 / (1 + \exp (- E4))$ (46)

$E5= \ 5.0394\ p_{wrn} + - 0.2975\ v_{tipn} + 14.9519$

$F5=1 / (1 + \exp (- E5))$ (47)

$E6= \ 0.0156\ p_{wrn} + 28.2183\ v_{tipn} + 1.5785$

$F6=1 / (1 + \exp (- E6))$ (48)

$E7= - 3.9918\ p_{wrn} + - 0.4473\ v_{tipn} \ - 14.5021$

$F7=1 / (1 + \exp (- E7))$ (49)

$E8= - 40.0445\ p_{wrn} + 1.1883\ v_{tipn} + - 68.8623$

$F8=1 / (1 + \exp (- E8))$ (50)

$D_n=1e+3*[.0025F1+2.0159F2+1.0774F3-2.6808F4 +.0043F5-1.6339F6-.9404F7-.0001F8-0.3875]$ (51)

L_{stackn}=1e+3*[.0025F1+2.0159F2+1.0775F3-2.6809 F4+.0049F5-1.6340F6-.9394F7-.0001F8-.3880] (52)

$Speed_{rpmn}$=1e3*[-.0098F1-.1763F2-.3387F3+0.8503 F4-1.4339F5+.5200F6-1.7635F7+.0051F8 + 1.1000] (53)

The un- normalized out puts

D ≅ 1.0e+004*0.00001 D_n+1.0e+4*0.00001 (54)

L_{stack} ≅1.0e+005*0.00001L_{stackn}+1.0e+4*0.00001(55)

$Speed_{rpm}$=1.0e+004*[7.5902$Speed_{rpmn}$+8.5608] (56)

5.2 ANN Geometric Model

Using the same technique also to implement a neural network unit, this model represents the relations between the required output power and tip speed values as inputs, and Armature Conductor Length, Armature Conductor Area, Mass of Armature Conductor, Overall Machine Length, Core inside Radius, Core outside Radius, Overall Diameter, Back Iron Mass, Teeth Mass, Core Mass, Magnet Mass, Shaft Mass, Service Mass, and Total Mass as outputs or targets. This model is done with two layers; hidden (contains 8 Neurons) and output (contains 14 Neurons).

E1= 0.7536 p_{wrn} + - 0.9363 v_{tipn} + - 0.8555

F1=1 / (1 + exp (- E1)) (57)

E2= - 0.6266 p_{wrn} + 2.8366 v_{tipn} + 5.4163

F2=1 / (1 + exp (-E2)) (58)

E3= 0.4195 p_{wrn} + - 29.4459 v_{tipn}+ 21.5276

F3=1 / (1 + exp (- E3)) (59)

E4= - 0.7413 p_{wrn} + 0.9804 v_{tipn} + 0.8277

F4=1 / (1 + exp (- E4)) (60)

E5= 0.7308 p_{wrn} + -1.0281 v_{tipn} + - 0.8013

F5=1 / (1 + exp (- E5)) (61)

E6= - 0.0765 p_{wrn} + - 1.7066 v_{tipn} + - 8.8790

F6=1 / (1 + exp (- E6)) (62)

E7= - 4.3547 p_{wrn} + - 0.4022 v_{tipn} + - 14.9932

F7=1 / (1 + exp (- E7)) (63)

E8= 0.5739 p_{wrn} + - 0.1087 v_{tipn} + 6.8954

F8=1 / (1 + exp (- E8)) (64)

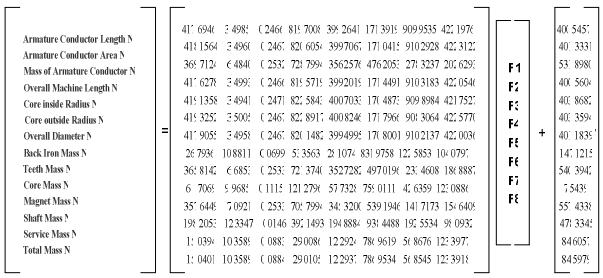

(65)

The un- normalized out puts

Armature Conductor Length ≅ 2.6097 Armature Conductor Length $_N$ + 7.2429 (66)

Armature Conductor Area ≅ 0.00001 Armature Conductor Area $_N$ + 0.00001 (67)

Mass of Armature Conductor ≅ 1.4681 Mass of Armature Conductor $_N$ + 2.1821 (68)

Overall Machine Length ≅ 0.0825 Overall Machine Length $_N$ + 0.1959 (69)

Core inside Radius ≅ 0.0140 Core inside Radius $_N$ + 0.0617 (70)

Core outside Radius ≅ 0.0173 Core outside Radius $_N$ + 0.0685 (71)

Overall Diameter ≅ 0.0346 Overall Diameter $_N$ + 0.1370 (72)

Back Iron Mass≅5.7121Back Iron Mass$_N$+4.7101(73)

Teeth Mass ≅ 1.6576 Teeth Mass $_N$ + 2.1698 (74)

Core Mass ≅ 7.3466 Core Mass $_N$ + 6.8799 (75)

Magnet Mass ≅ 2.1731 Magnet Mass $_N$ + 2.6088 (76)

Shaft Mass ≅ 7.5460 Shaft Mass $_N$ + 5.3404 (77)

Service Mass ≅ 2.7693 Service Mass $_N$ + 2.5517 (78)

Total Mass ≅ 21.2311 Total Mass $_N$ + 19.5627 (79)

5.3 ANN Electric and Performance Model

Using the same technique to implement a neural network unit, this model represents the relations between the required output power and tip speed values as inputs, and Magnetic Flux Density, Magnetic Flux, Internal Voltage, Air Gap Inductance, Slot Leakage Inductance, Total Inductance, Reactance, Stator Resistance, Tooth flux Density, Back Iron flux Density, Teeth Loss, Core Back Iron Loss, Total Core Loss, Terminal Voltage, Armature Current, Windage Loss, Conductor Loss, Total Losses, and Efficiency as outputs or targets. This model is done with two layer hidden (contains 9 Neurons) and output (contains 19 Neurons).

E1= -1.1677 p_{wrn} + 3.1774 v_{tipn} + 6.2314

F1=1 / (1 + exp (- E1)) (80)

E2= 0.0210 p_{wrn} + - 0.2037 v_{tipn} + 2.3044

F2=1 / (1 + exp (- E1)) (81)

E3= - 0.0283 p_{wrn} + 0.1771 v_{tipn} + -3.6837

F3=1 / (1 + exp (- E1)) (82)

E4= -0.0611 p_{wrn} + -0.0824 v_{tipn} + -3.8055

F4=1 / (1 + exp (- E1)) (83)

E5= -1.7672 p_{wrn} + 0.0953 v_{tipn} + -4.8035

F5=1 / (1 + exp (- E1)) (84)

E6= 0.1549 p_{wrn} + 0.8839 v_{tipn} + 7.5520

F6=1 / (1 + exp (- E1)) (85)

E7= - 0.4985 p_{wrn} + - 0.9817 v_{tipn} + -8.1450

F7=1 / (1 + exp (- E1)) (86)

E8= 11.7121 p_{wrn} + - 0.0279 v_{tipn} + 23.3795

F8=1 / (1 + exp (- E1)) (87)

E9= - 11.6468 p_{wrn} + 0.0395 v_{tipn} + -24.4962

F9=1 / (1 + exp (- E1)) (88)

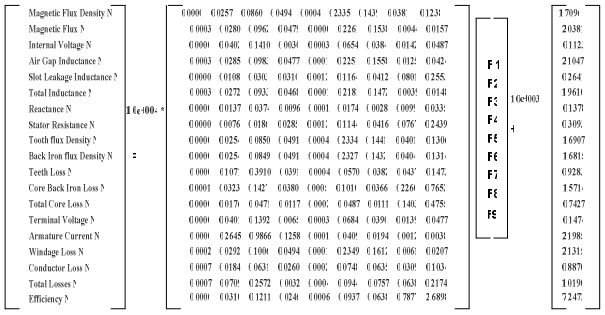

(89)

The un- normalized out puts

Magnetic Flux Density ≅1.0e+003 * (0.00001 Magnetic Flux Density $_N$ + 0.0009) (90)

Magnetic Flux ≅ 1.0e+003 *(0.0001 Magnetic Flux $_N$ + 0.0001) (91)

Internal Voltage ≅ 1.0e+003 * (0.2990 Internal Voltage $_N$ + 0.7170) (92)

Air Gap Inductance ≅ 1.0e+003 * (0.00001 Air Gap Inductance $_N$ + 0.00001) (93)

Slot Leakage Inductance ≅ 1.0e+003 * (0.00001 Slot Leakage Inductance $_N$ + 0.00001) (94)

Total Inductance≅ 1.0e+003 * (0.00001 Total Inductance $_N$ + 0.00001) (95)

Reactance≅1e3*(.0001 Reactance $_N$ + 0.0002) (96)

Stator Resistance ≅ 1.0e+003 * (0.00001 Stator Resistance $_N$ + 0.00001) (97)

Tooth flux Density ≅ 1.0e+003 * (0.00001 Tooth flux Density $_N$ + 0.0017) (98)

Back Iron flux Density ≅ 1.0e+003 * (0.00001 Back Iron flux Density $_N$ + 0.0012) (99)

Teeth Loss≅1e3*(.5014Teeth Loss $_N$+.7719) (100)

Core Back Iron Loss ≅ 1.0e+003 *(0.9307 Core Back Iron Loss $_N$ + 1.2276) (101)

Total Core Loss ≅ 1.0e+003 * (1.3425 Total Core Loss $_N$ + 1.9995) (102)

Terminal Voltage ≅ 1.0e+003 * (0.2943 Terminal Voltage $_N$ + 0.6870) (103)

Armature Current ≅ 1.0e+003 * (0.5855 Armature Current $_N$ + 0.5708) (104)

Windage Loss ≅ 1.0e+003 * (0.1116 Windage Loss $_N$ + 0.1429) (105)

Conductor Loss ≅ 1.0e+003 * (1.9786 Conductor Loss $_N$ + 1.2260) (106)

TotalLosses≅1e3(2.0062TotalLosses$_N$+3.7963) (107)

Efficiency≅1e3(.0001 Efficiency $_N$+.0010) (108)

6. Conclusions

The sizing method presented gives a step by step method for high frequency PM generator design. This paper illustrates the benefits of HFPM generators, compared to the original PM synchronous generators, since it offers significant reductions in both weights and volumes. It discusses the electrical and magnetic sizing of HFPMGs, within the power range of 5:500 Kw and tip speed in the range of 50:250 m/s. Finally, three neural networks with their algebraic equations are deduced to be used for predicting any value in these ranges over the 3D graphs as shown in this paper.

References

1. Ahmad, R. A., Pan, Z., and Saban, D. M., "On-Board Electrical Network Topology Using High Speed Permanent Magnet Generators," Electric Ship Technologies Symposium, 2007. ESTS apos;07. IEEE Volume , Issue , 21-23, pp.356 – 362, May 2007.
2. Scridon, S., Boldea, I., Tutelea, Blaabjerg, L., F., and Ritchie, E., "BEGA – A Biaxial Excitation Generator for Automobiles: Comprehensive Characterization and Test Results," IAS, 2004, Industry Applications Conference, 2004. 39th IAS Annual Meeting Conference Record of the 2004 IEEE, vol.3, pp. 1682 – 1690, 3-7 Oct. 2004.
3. Binder, A., Schneider, T., and Klohr, M., "Fixation of Buried and Surface- Mounted Magnets in High-Speed Permanent-Magnet Synchronous Machines," IEEE Trans. On Industry Applications, Vol. 42, NO. 4, pp. 1031 – 1037, July/August, 2006.
4. Hosseini, S. M., Mirsalim, M. A., and Mirzaei, M. , "Design, Prototyping, and Analysis of a Low Cost Axial-Flux Coreless Permanent-Magnet Generator," IEEE Trans. On Mag., Vol. 44, No. 1, pp. 75 – 80, Jan. 2008.
5. Mellor, P.H., Burrow, S.G., Sawata, T., and Holme, M., "A Wide – Speed – Range Hybrid Variable – Reluctance / Permanent – Magnet Generator for Future Embedded Aircraft Generation Systems," IEEE Trans. On Industry App.,Vol. 41, No. 2,PP. 551–556, March/April 2005.
6. Sadeghierad, M., Lesani, H., Monsef, H., and Darabi, A., "Design considerations of High Speed Axial Flux permanent magnet Generator with Coreless Stator," The 8th International Power Engineering Conference (IPEC), pp. 1098 – 1102, 2007.
7. Arnold, D. P., Das, S., Park, J. W., Zana, I., Lang, J. H., and Allen, M. G., "Micro fabricated High-Speed Axial-Flux Multi watt Permanent- Magnet Generators—Part II: Design, Fabrication, and Testing," Journal Of Micro Electromechanical Systems, Vol. 5, No. 5, pp. 1351 – 1363, October 2006.
8. Paulides, J. J. H., Jewell, G. W., and Howe, D., "An Evaluation of Alternative Stator Lamination Materials for a High – Speed, 1.5 MW, Permanent Magnet Generator," IEEE Trans. On Magnetics, Vol. 40, No. 4, pp. 2041 – 2043, July 2004.
9. Jang, S. M., Cho, H. W., and Jeong, Y. H., "Influence on the rectifiers of rotor losses in high – speed permanent magnet synchronous alternator," Journal of Applied Physics, 08R315, American Institute of Physics, 08R315-1 - 08R315-3, 2006.
10. Kolondzovski, Z., "Determination of critical thermal

operations for High – speed permanent magnet electrical machines," The International Journal for Computation and Mathematics in Electrical and Elect. Eng., Vol. 27 No. 4, pp. 720-727, 2008.
11. Nagorny, A. S., Dravid, N. V., Jansen, R. H., and Kenny, B. H., "Design Aspects of a High Speed Permanent Magnet Synchronous Motor / Generator for Flywheel Applications," NASA/TM—2005-213651 June 2005, International Electric Machines and Drives Conference sponsored by the IEEE Ind. Appl. Society, IEEE Power Elect. Society, IEEE Power Eng. Society, and IEEE Ind. Elect. Society, San Antonio, Texas, May 15–18, 2005.
12. Hanselmann, D. C., Brushless Permanent Magnet Motor Design, New York: McGraw- Hill, 1994.
13. Hendershot, J. R. and Miller, T. J. E., Design of Brushless Permanent Magnet Motors, Oxford, U.K.: Magna Physics Publishing and Clarendon Press, 1994.
14. Rucker, J. E., Kirtley, J. L., McCoy, Jr. T. J., "Design and Analysis of a Permanent Magnet Generator For Naval Applications," IEEE Electric Ship Technologies Symposium, pp. 451 – 458, 2005.
15. Kang, D., Curiac, P., Jung, Y., and Jung, S., "Prospects for magnetization of large PM rotors: conclusions from a development case study," IEEE trans. On Energy Conversion, vol. 18, no. 3, Sept. 2003.
16. Paulides, J., Jewell, G., and Howe, D., "An evaluation of alternative stator lamination materials for a high speed, 1.5 MW, permanent Magnet Generator," IEEE Trans. On Magnetics, vol. 40, no. 4, July 2004.
17. Bianchi, N., and Lorenzoni, A., "Permanent magnet generators for wind power industry: an overall comparison with traditional generators," Opportunities and advances in international power generation, conference publication No. 419, 1996.
18. Rahman, M. A., and Slemon, G. R., "Promising Applications of Neodymium Iron Boron Iron Magnets in Electrical Machines," IEEE Trans. On Magnetics, Vol. No. 5, Sept 1985.
19. Polinder, H. and Hoeijmakers, M. J., "Eddy – Current Losses in the Segmented Surface Mounted Magnets of a PM Machine," IEE Proceedings, Electrical Power Applications, Vol. 146, No. 3, May 1999.
20. Aglen, O., and Andersson, A., "Thermal Analysis of a High Speed Generator," Industry Applications Conference, 2003. 38th IAS Annual Meeting. Con. vol.1, pp. 547- 554, 12-16 Oct. 2003. Current Version Published: 2004-01-07 IEEE Transactions, 2003.
21. Pepi, J., and Mongeau, P., " High power density permanent magnet generators," DRS Electric power technologies, Inc., 2004.
22. Rubaai A., Koteru R., Kankam M. D.: A continually online-trained neural network controller for brushless dc motor drives. IEEE Trans. on Industry Applications, vol. 36, no. 2, 2000, pp. 475-483.
23. Arzu Sencan, Kemal A.Yakut, Soteris A.Kalogirou: Thermodynamic analysis of absorption systems using artificial neural network. Renewable Energy, Volume 31, issue 1, Jan. 2006, pages 29 – 43.
24. A. El Shahat, "Generating Basic Sizing Design Regression Neural Function for HSPMSM in Aircraft" EP-127, 13th International Conference on Aerospace Science & Aviation Technology, May 26 – 28, 2009, ASAT 2009 – Military Technical College, Cairo, Egypt.
25. El Shahat, A and El Shewy, H, "Neural Unit for PM Synchronous Machine Performance Improvement used or Renewable Energy", Ref: 93, The Third Ain Shams University International Conference on Environmental Engi. (Ascee- 3), April 14-16 2009, Cairo, Egypt.
26. A. El Shahat, and H. El Shewy, "Neural Unit for PM Synchronous Machine Performance Improvement used for Renewable Energy", Paper Ref.: 910, Global Conference on Renewable and Energy Efficiency for Desert Regions (GCREEDER2009), Amman, Jordan.
27. A. El Shahat, and H. El Shewy, "PM Synchronous Motor Control Strategies with Their Neural Network Regression Functions", Journal of Electrical Systems, Vol. 5, Issue 4, Dec. 2009.